Identification and High-Accuracy Range Estimation With Doppler Tags in Radar Applications

Theresa Antes, *Graduate Student Member, IEEE*, Paul Schubert, Thomas Zwick, *Fellow, IEEE*, and Benjamin Nuss, *Senior Member, IEEE*

***Abstract*— Radar sensors are widely used to support further system automation as they reliably provide range, velocity, and angle information for multiple objects. Nevertheless, unique identification of an object is not within the typical function range of radar; often, supportive systems are required. To overcome this limitation, a multipurpose tag concept for fast chirp frequency-modulated continuous wave (FC-FMCW) radar is introduced. The Doppler tag applies an artificial frequency shift following the Doppler phenomenon for unique identification of tagged objects with conventional radar hardware. It enables simultaneous detection and feature estimation of tagged and untagged objects. The idea of the Doppler tag is presented together with a realization and the required signal processing to allow for identification and high-accuracy range estimation. Simulations and measurements are provided to support the overall understanding and prove the functionality of the radar-tag system.**

***Index Terms*— Doppler tag, fast chirp frequency-modulated continuous wave (FC-FMCW), high-accuracy range estimation, identification, radar sensing.**

I. Introduction

In an industrial context, radar sensors can deliver the data basis that enables further automation by providing necessary data about the vicinity. Optical systems may be prone to failure, whereas radar sensors offer a robust and reliable solution in challenging lighting conditions, even in the presence of dust or smoke. Hence, they are used in a multiplicity of tasks in that context, such as hidden object detection, distance measurement, or positioning [1], [2], [3]. For multiple distributed objects, the unique identification of an object is of interest to obtain an orientation in the environment or pinpoint the object of interest among several targets. Radar sensors can deliver information about range, angle, motion, and radar cross section (RCS) of a target, but identification additionally requires extensive knowledge about the surroundings to infer from this information to the object itself. As an alternative, radar tags can take on identification and interoperate with radar sensors, exploiting the associated advantages [4], [5].

Received 23 August 2024; revised 23 October 2024 and 8 January 2025; accepted 11 January 2025. Date of publication 16 January 2025; date of current version 29 January 2025. This work was supported by the German Research Foundation (DFG) through the Project "DoSIS" under Grant 533282729. *(Corresponding author: Theresa Antes.)*

Theresa Antes, Thomas Zwick, and Benjamin Nuss are with the Institute of Radio Frequency Engineering and Electronics (IHE), Karlsruhe Institute of Technology (KIT), 76131 Karlsruhe, Germany (e-mail: theresa.antes@kit.edu).

Paul Schubert is with Siemens AG, 76187 Karlsruhe, Germany.

Digital Object Identifier 10.1109/TRS.2025.3530560

A common approach is that harmonic tags are used to identify objects otherwise hidden or showing insufficient RCS to be differentiated from the surroundings [6], [7]. They not only require a tag but also a tailored radar transceiver, differing from the common hardware by a frequency multiplication between the transmit and receive paths. With a few exceptions, e.g., [8], simultaneous radar sensing of tagged and untagged objects is not possible with these radars, which impedes a comprehensive supervision of complex scenarios. Furthermore, tags can only be distinguished from their environment but not from each other, as typically only a single harmonic frequency is evaluated. Hence, differentiation of multiple tagged objects and, therefore, real identification is not possible using harmonic tags. For this reason, harmonic tags are well-suited for scenarios where the goal is to detect and potentially track a specific kind of target, but not for overall monitoring of intricate environments as often demanded in an industrial setting.

Similar to harmonic tags, other principles of clutter-suppressing tags are discussed, enabling identification and radar sensing only for tagged objects [9], [10], [11]. Furthermore, the combination of modulation with enhanced antenna systems such as Van Atta arrays is possible to enhance the tag operation [12]. Another approach is code-based tags, which combine identification and radar sensing with the exchange of information about the object. Modulated backscattering tags enable, e.g., communication with frequency-modulated continuous wave (FMCW) [13] or synthetic aperture radars [14]. Active and passive reflector tags are considered in [15], [16], and [17]. Similarly, passive, frequency-coded landmarks are proposed, e.g., in [18] and [19]. Beside radar tags, a variety of tag technologies not relying on radar, such as the widely used barcode or ultra wide-band (UWB) tags, are available, which all come with their own tag and corresponding reader architecture. For UWB, ranging information is available; however, most tag technologies only offer identification.

Much more information about the identified object can be obtained using a radar sensor. Particularly, high accuracy in range estimation is favorable and, for some applications, even essential. Furthermore, the possible motion of the object is to be detected and quantified. For these requirements, fast chirp FMCW (FC-FMCW), also referred to as fast chirp sequence, is a promising modulation scheme. Coming from the well-established FMCW, FC-FMCW additionally allows for the

separation of multiple targets in range and velocity while preserving a similar processing gain. High-accuracy range estimation is possible by evaluating the phase offset in addition to the common frequency-based analysis, an approach introduced for FMCW [20] but transferable to FC-FMCW [21], also including Doppler shifts [22]. Using adequate signal processing, high accuracy is achieved without the need for complex and costly hardware.

This article introduces a new tag concept tailored to FC-FMCW, the Doppler tag. The concept includes an advanced signal processing chain and a relatively simple hardware approach that is tailored precisely to the intended functionality and processing, enabling the identification and highly accurate range estimation of a tag while simultaneously being receptive to untagged surroundings. The tag emulates the Doppler phenomenon and, by using different identification frequencies, allows for unique identification of tagged objects with conventional radar hardware. Classical radar sensing is not impaired and can be applied to both tagged and untagged objects. The focus is on robust object identification and the particularly challenging high-accuracy range estimation, which requires unimpaired phase information despite the modulation applied by the tag. To meet the requirements enabling this estimation, both hardware and processing have to be carefully designed and coordinated. Similar hardware approaches for radar tags exist; however, different design priorities lead to tags with distinct characteristics and features. In [23] and [24], switching between modulation frequencies allows for communication. The used frequencies are considerably higher than motion-caused Doppler shifts that are mimicked with the Doppler tag, so that coupling terms become significant and processing is not alike. Appropriate signal processing is essential for the Doppler tag and consists of well-established processing steps and new elements that, only in combination, provide the desired information. The proposed concept of hardware and signal processing to achieve unique object identification and high-accuracy range estimation using a simple tag setup and common radar hardware with simultaneous classical radar sensing distinguishes the Doppler tag from other approaches.

The resultant system simultaneously produces an overview image of its surroundings and high-accuracy measurements of certain points where the tags are located. Thereby, it can enable other systems to work by providing necessary data about the common vicinal area, hence being the eye of an autonomous environment. A variety of applications can be found wherever the autonomy of systems or subsystems is intended or is to be supported with additional information. Particularly, the industrial and medical sectors can benefit, where identification and localization of certain objects of interest are crucial. The Doppler tag concept is of special interest in contexts where identification is required jointly with a highly accurate range estimate of the tagged objects. However, it is not limited to a certain application or field of use. For example, a robot co-worker independently identifies tools or objects to proceed with, as shown in Fig. 1. Due to the high accuracy of range estimation, the items can be grabbed and handled precisely. An autonomously calibrating robot arm could streamline the recalibration process by approaching a Doppler tag at a known position and accurately estimating the distance, thereby eliminating the need for time-consuming manual recalibration. In addition to the high range estimation accuracy, the usage of common radar hardware, which is already provided for classical sensing, is of advantage as no secondary system has to be installed. When approaching a Doppler tag, wake-up functionalities can enable the start of object-specific sensing or processing tasks. The unmodified radar hardware is essential here as it is required for subsequent functionalities, for which the tag only provides a trigger. Using Doppler tags as reference points, autonomous mobile devices could orient themselves without optical markers or guiding wires prone to damage. In this application, the unique combination of features of the Doppler tag is particularly beneficial. The straightforward tag hardware facilitates compact and low-cost fabrication so that a large number of tags can be used. The accuracy of range estimation for multiple, uniquely distinguishable tags enables robust and reliable positioning, while classical radar sensing equips the robot with an overview of its surroundings, enabling further sensing and preventing collisions.

Fig. 1. Exemplary application of a Doppler tag for object identification.

The basic idea and principles of the Doppler tag, together with substantiating measurements, are presented to introduce the new concept. The remainder of this article is organized as follows. Section II discusses the idea of the Doppler tag and its realization as well as the system and processing model of FC-FMCW including a Doppler tag. Section III introduces the measurement setup and presents and contextualizes the conducted measurements in terms of identification and high-accuracy range estimation. Finally, concluding remarks are given in Section IV.

II. Concept of Doppler Tags

The idea of the Doppler tag is to use an artificially raised Doppler shift for identification of a tagged object. Each artificial Doppler shift is characteristic of the tagged object of interest, which allows for unique identification. In FMCW or FC-FMCW radar, a Doppler shift is just a shift in frequency, which the tag introduces by means of mixing. In the most basic setup, the radar signal is received at the tag, mixed with

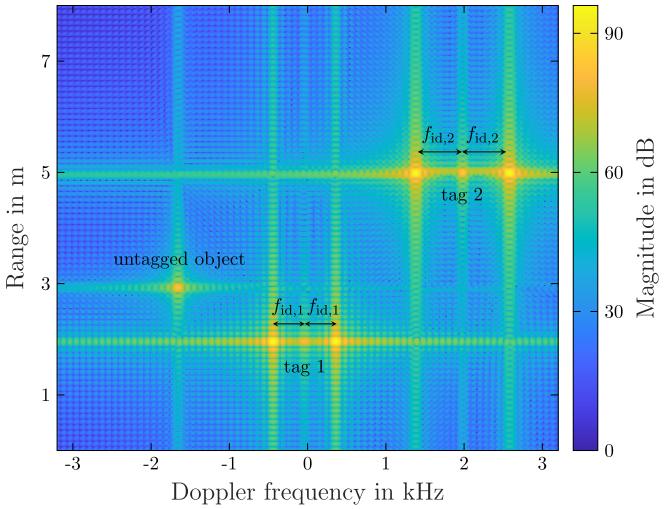

Fig. 2. Simulated range-Doppler map for three objects. The two objects at 2 and 5 m are tagged with $f_{\mathrm{id},1} = 400$ Hz and $f_{\mathrm{id},2} = 600$ Hz, respectively. While the first one is static, the second one moves with 5 m s^{-1} ($f_{D,2} \approx 2$ kHz). The third object does not carry a Doppler tag but moves with -4 m s^{-1} ($f_{D,3} \approx -1.6$ kHz), starting at 3 m.

a certain identification frequency f_{id} and transmitted back in the direction of the radar. Only a frequency shift is applied, but no change in range occurs, so no real motion is emulated. The artificial Doppler is in the same order of magnitude as a motion-caused Doppler shift, so only small modifications in the processing chain are necessary. In contrast to most other radar tags, modification of the radar hardware is not necessary to allow for operation together with Doppler tags. Instead, identification is achieved solely through signal processing, similar to standard Doppler determination. It can be carried out in parallel to normal sensing of the environment so that tagged and untagged objects are both detected, e.g., within a range-Doppler map. Fig. 2 shows the resulting range-Doppler map for the simulation of two Doppler tags with $f_{\mathrm{id},1} = 400$ Hz and $f_{\mathrm{id},2} = 600$ Hz as well as an untagged object moving with $v = -4$ m s^{-1}, corresponding to a Doppler shift of $f_{D,3} = -1.6$ kHz. Tagged objects are detected twice, once with a certain artificial Doppler shift, leading to two peaks, and once at their real velocity, as the radar signal is reflected off the object itself without passing through the tag. Using an active amplification within the tag, the amplitude of the tag response is significantly above that of the object reflection. The mixing products are visible as two peaks at $f_D \pm f_{\mathrm{id}}$ due to real-valued mixing. Untagged objects are detected as normal. However, they do not disturb tag identification as they are mostly static and, if not, unlikely to have the exact same Doppler shift as applied by a tag. Using real-valued mixing, tags can be distinguished even from objects with the same velocities as further discussed in Section II-A. Masking of untagged objects by a tag is possible while range and velocity bins are very similar or even equal. However, this is rarely the case in real scenarios and only a short-time effect, as the required motion of the untagged object will move it to a different range bin and resolve the ambiguity.

As the tags are separated by their artificial Doppler frequency f_{id}, the number of simultaneously usable tags is limited by the velocity resolution and maximum unambiguous velocity

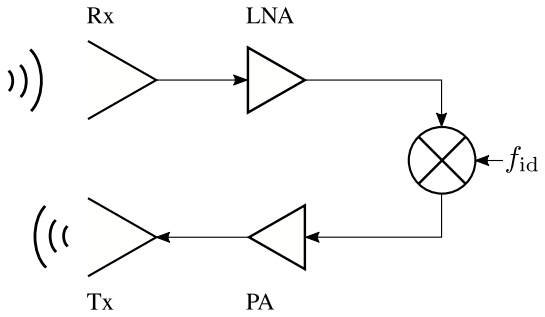

Fig. 3. Block diagram of a realization of the Doppler tag using real-valued mixing.

of the radar. In theory, each Doppler bin could be occupied with one tag, allowing a number of tags equal to the number of chirps per measurement if complex-valued tag mixing is used and complex raw data are available. Nonetheless, some margin should be allowed in practice to prevent false identification as soon as the Doppler determination is off by one bin or the tagged object additionally is in motion. Generally, the available number of tags is dependent on the number of chirps per measurement, the size of the margin that is granted between two tags, the potential velocities of the tagged objects, and the realization of the mixing process and has hence to be determined for each targeted application.

Doppler tags are a suitable solution, in particular when highly accurate range estimation, despite all tag functionalities, is required. Possible applications range from low-level supervision to autonomous localization tasks and can exploit the benefits of Doppler tags to different extents. The radar parameters, such as bandwidth, measurement time, and number of chirps, are to be chosen depending on the targeted accuracy of range and real Doppler estimation as well as the required number of tags. If positioning is aimed at, the number and distribution of tags additionally influence the achievable position accuracy. The tag design itself can be optimized for a specific application, e.g., adding additional amplification for particularly high measurement ranges or special antenna constellations for high directivity. As the presented Doppler tag idea is not based on a distinct application, a basic tag realization is proposed hereinafter, enabling all discussed functionalities but not being optimized to a certain scenario.

A. Doppler Tag Realization

The block diagram of a realization of the Doppler tag with real-valued mixing is shown in Fig. 3. The signal transmitted by an FC-FMCW radar is received at the Doppler tag receiver (Rx) and amplified using a low-noise amplifier (LNA). A real-valued mixer applies a frequency shift to the signal, where f_{id} is the characteristic shift frequency used for identification of the tagged object. The assignment of frequencies $f_{\mathrm{id},x}$ to objects x is to be known. Due to the random phase position of the mixing signal relative to the radar signal, mixing applies an unknown phase shift to the signal in addition to the intended frequency shift, which is irrelevant for identification but influences the possibilities for high-accuracy range estimation. Using a real-valued mixer, both sidebands are included in the signal, and the phase shift can be canceled,

although unknown, as will be further discussed in Section II-B. In addition, untagged but moving objects can be distinguished from tagged ones as the complete signal is shifted by their velocity-generated Doppler frequency without sidebands from mixing. From the identification point of view, complex mixing provides more available tag frequencies as $\pm f_{\mathrm{id}}$ can be used to tag two objects, but the phase shift cannot be eliminated. Additionally, if the tagged object is in motion, symmetric guard intervals around the artificial Doppler are necessary to prevent erroneous identification. A real Doppler shift adds or subtracts from the artificial one, depending on the relative direction of motion. This displacement within the Doppler domain has to happen within a distinct interval where all frequencies belong to one object; otherwise the real Doppler will falsify the object identification. This does not apply for real-valued mixing as the identification frequency is determined by the frequency difference between the two sidebands. A real Doppler shift changes the position of both sidebands; their position relative to each other, and hence the determined f_{id}, does not change. A corrupted identification of moving untagged objects as tagged ones or a confusion of Doppler tags is hence unlikely and can be further prevented by scenario-aware choices of $f_{\mathrm{id},x}$. The focus of this work is on the Doppler tag and its influence on range estimation; thus, only real-valued mixing is considered hereinafter. The frequency-shifted signal is optionally amplified again using a power amplifier (PA) and retransmitted toward the radar via the Tx antenna. An exemplary Doppler tag setup using waveguide components will be introduced in Section III. As the shift in frequency is small relative to the center frequency of the radar, the tag response is received at the radar together with and in the same way as the reflections of untagged objects in the radar field of view. It can, therefore, be easily integrated into the FC-FMCW system model and evaluated using standard radar signal processing.

B. System and Processing Model Including a Doppler Tag

The processing chain for a Doppler tag from identification to range and velocity estimation is shown in Fig. 4 and discussed hereinafter, starting from the system model.

The transmitted radar signal consists of N_{sample} samples per chirp and N_{chirp} chirps of duration T that start at a frequency f_{min} and cover a bandwidth B, each. Omitting the amplitude, the signal can be represented by its phase Φ_{tx} as $s_{\mathrm{tx}}(t,m) = e^{j\Phi_{\mathrm{tx}}(t,m)}$, where $m \in [0, N_{\mathrm{chirp}} - 1]$ is the slow time index, and $t \in [0, T]$ is the fast time. Considering a sawtooth modulation, the transmitted phase over all chirps can be determined from the required linear frequency curve by integrating it

$$\Phi_{\mathrm{tx}}(t,m) = 2\pi\left(f_{\mathrm{min}}t + \frac{B}{2T}t^2 + \left(f_{\mathrm{min}} + \frac{B}{2}\right)mT\right). \quad (1)$$

The first two summands describe the current chirp, and the m-dependent summands describe the chirps already passed, neglecting idle times between them.

Due to the delay τ, the phase of the received signal is shifted in time toward the phase of the transmitted signal as

$$\Phi_{\mathrm{rx}}(t,m) = \Phi_{\mathrm{tx}}(t-\tau, m). \quad (2)$$

In general, this delay is dependent on the initial target range at the beginning of a measurement R_0, resulting in a delay τ_0, and the velocity of the target v. Under the assumption of a constant velocity, the time-dependent delay $\tau(t,m)$ is

$$\tau(t,m) = \frac{2R(t,m)}{c_0} = \tau_0 + \frac{2v}{c_0}\cdot(t+mT) \quad (3)$$

where c_0 is the speed of light in free space. To determine the initial target range R_0 and velocity v, the phase of the beat signal is evaluated using (1)–(3)

$$\begin{aligned}\Phi_{\mathrm{b}}(t,m) &= \Phi_{\mathrm{tx}}(t,m) - \Phi_{\mathrm{rx}}(t,m)\\ &= 2\pi\left(\left(\frac{B}{T}\tau_0\left(1-\frac{2v}{c_0}\right) + f_{\mathrm{min}}\frac{2v}{c_0}\right)t\right.\\ &\quad + \left(\frac{2v}{c_0}\left(f_{\mathrm{min}} - \frac{B}{T}\tau_0\right)\right)mT\\ &\quad + \left(\frac{B}{T}\frac{2v}{c_0}\left(1-\frac{2v}{c_0}\right)\right)tmT\\ &\quad + \left(\frac{B}{T}\frac{2v}{c_0}\left(1-\frac{v}{c_0}\right)\right)t^2\\ &\quad + \left(-\frac{B}{T}\frac{2v^2}{c_0^2}\right)(mT)^2\\ &\quad \left. + \tau_0\left(f_{\mathrm{min}} - \frac{B}{2T}\tau_0\right)\right). \end{aligned} \quad (4)$$

In this form, the signal model represents only the part of the signal that will be sampled and used for signal processing afterward. This is the case when both the transmit and receive signals are present for the mixing process, while the parts at the beginning and end of the ramp are omitted, hence $\tau \ll T$ and $B \ll f_{\mathrm{min}}$. An IQ-mixer is required in the radar Rx chain to avoid the occurrence of a second sideband at the negative Doppler frequency, which would cause additional spectral components and impair both identification and high-accuracy range estimation.

If the target carries a Doppler tag as discussed in Section II-A, an additional frequency shift of type $2\pi f_{\mathrm{id}}(t + mT)$ is applied through mixing. This artificial shift is not analogous to a Doppler shift originating from the real motion of a target with velocity v, as the range does not change over time due to this shift. Hence, only the phase within each chirp is altered, and neither migration over range or Doppler bins nor range Doppler coupling occurs as is the case for a moving target [25]. Using real-valued mixing, two mixing products emerge, and the final beat signal can mathematically be described as the sum of those, hence

$$\begin{aligned}s_{\mathrm{b}}(t,m) = {} & e^{j\Phi_{\mathrm{b}}(t,m) + j(2\pi f_{\mathrm{id}}(t+mT)+\varphi_{\mathrm{id}})}\\ & + e^{j\Phi_{\mathrm{b}}(t,m) - j(2\pi f_{\mathrm{id}}(t+mT)+\varphi_{\mathrm{id}})}. \end{aligned} \quad (5)$$

In (5), not only a frequency shift is applied but an additional, unknown phase shift φ_{id} originating from the random phase position of the mixing signal. Equation (5) together with (4) describes the complete signal model for an FC-FMCW radar signal received and retransmitted by a Doppler tag with real-valued mixing. In this investigation, the focus should be on the Doppler tag and its influence on range estimation. Therefore,

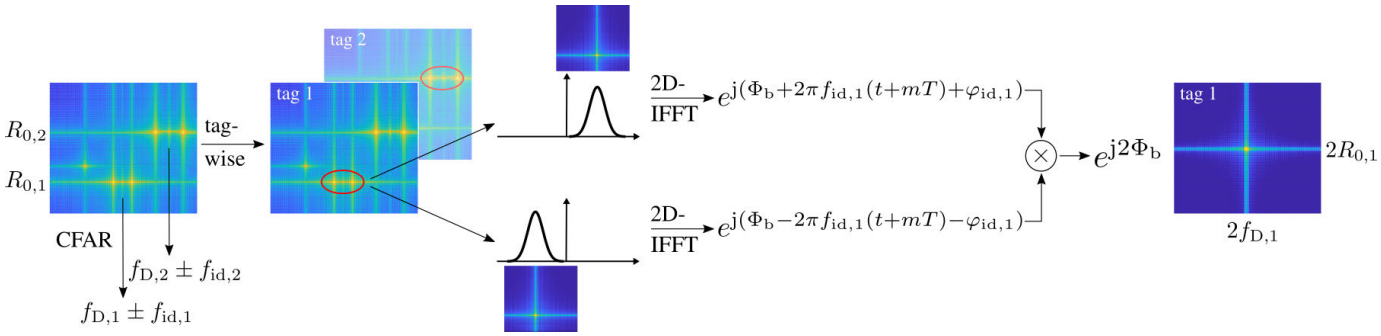

Fig. 4. Processing chain for Doppler tag identification and removal of its influence for subsequent range and velocity estimation. The occurring tag frequencies $f_{id,x}$ are determined from a range-Doppler map, and the remaining processing is done tag-wise. Windowing simultaneously separates one tag from the other targets and the two sidebands of this tag from each other. The two windowed signals are multiplied in the time domain to eliminate the influence of the Doppler tag in frequency and phase. The resulting signal contains only the information about one tagged object and therefore allows for conventional processing. However, the phase is doubled due to the preceding multiplication, which consequently results in a doubling of the range and velocity estimates and must be accounted for in further processing.

only static scenarios are considered hereinafter, and the beat signal phase (4) can be simplified with $v = 0\ \mathrm{m\,s^{-1}}$.

Applying this model in simulations, a range-Doppler map as shown on the very left of Fig. 4 and in Fig. 5(a) is obtained. In the latter, a single static target is simulated at a range of $R = 2$ m, carrying a Doppler tag with $f_{id} = 5$ kHz, at $f_{min} = 60$ GHz corresponding to $\approx$12.5 $\mathrm{m\,s^{-1}}$. The mixing products are visible at $\pm f_{id}$ due to real-valued mixing. The object reflection without tag is not included in this simulation. Since the artificial Doppler shift f_{id} does neither imply any change in range nor a spread over multiple Doppler bins, the target is sharply defined. Fig. 5(b) shows the range-Doppler map from an exemplary measurement (Section III) of a similar scenario. The tag, the object reflection, and multiple reflections between radar and tag at multiples of the target range R are visible. In addition to the tag peaks at $\pm f_{id}$, peaks at multiples of f_{id} occur, which originate from multiple reflections traveling through the tag more than once. The obligatory static measurement surrounding is visible at 0 Hz and spreads over multiple range bins.

Signal processing is performed in two steps: first, identifying the target by means of f_{id}, and second, determining the initial target range R_0. f_{id} is obtained from a 2-D fast Fourier transform (FFT) on the radar signal and a subsequent maximum search or constant false alarm rate (CFAR) detection on the resulting range-Doppler map as shown in the left part of Fig. 4. For a single tagged object, two maxima are detected at $\pm f_{id}$ as also shown in Fig. 5. The objects in question are assumed to be preknown, such as from a table that assigns an f_{id} to each tagged object, so that unambiguous identification is possible from f_{id}. For more than one tagged object in the radar field of view, multiple maxima arise. Identification is possible from the symmetric pairs in the range-Doppler map, and untagged objects can be differentiated. All subsequent processing steps need to be completed for each tag separately. A single tag is hence assumed for the following explanations and the visualization in Fig. 4.

For undisturbed range estimation, the influence of the Doppler tag is to be eliminated. To achieve this, 2-D windowing is applied around each of the two maxima of a tag, simultaneously separating this tag from other targets and the two sidebands of this tag from each other. The two resulting signals are retransformed to the time domain using a 2-D inverse FFT (IFFT). Each signal now only carries the information of one sideband, and by means of a complex multiplication, the influence of the considered tag vanishes, resulting in

$$s_{b,w/o\,t}(t,m) = e^{j\Phi_b(t,m)+j(2\pi f_{id}(t+mT)+\varphi_{id})} \tag{6}$$

$$\cdot\, e^{j\Phi_b(t,m)-j(2\pi f_{id}(t+mT)+\varphi_{id})} \tag{7}$$

$$= e^{j2\Phi_b}. \tag{8}$$

This elimination is a key aspect of the proposed Doppler tag, as it enables high-accuracy range estimation based on a phase offset analysis despite the modifications the tag applied to the signal. As the enhancement in accuracy is achieved solely in signal processing, no demanding hardware requirements have to be met. However, a reasoned hardware design is essential to allow for the elimination and, subsequently, for high-accuracy range estimation. A related elimination processing is applied in [23], but the frequency usage is different due to different tag and radar architectures. Hence, the elimination is required to be able to estimate the object range from the peak separation, while for the Doppler tag, the tag influence is eliminated to allow for parameter estimation in the same way and with similar accuracy as for an untagged object.

The phase of the beat signal can, in the case of no motion [$v = 0\ \mathrm{m\,s^{-1}}$ in (4)] and no Doppler tag [using (7)], be simplified to

$$\Phi_{b,w/o\,t}(t,m) = 2\pi\left(\frac{B}{T}\tau_0 \cdot t + \underbrace{\tau_0\left(f_{min} - \frac{B}{2T}\tau_0\right)}_{\varphi_b}\right). \tag{9}$$

The resulting range-Doppler map is shown on the right side of Fig. 4 as well as in Fig. 6 with the comparison of simulation and measurement. After this processing step, there is a distinct map for each evaluated tag on which any further processing is performed. The doubling in phase, transferring to range and velocity, is a side effect of the multiplication as shown in (8) and can be corrected during estimation. In the phase

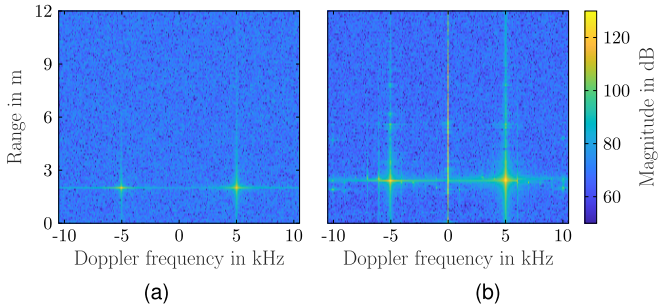

Fig. 5. Range-Doppler map of a single static target at 2 m distance, tagged with 5 kHz from (a) simulations and (b) measurements.

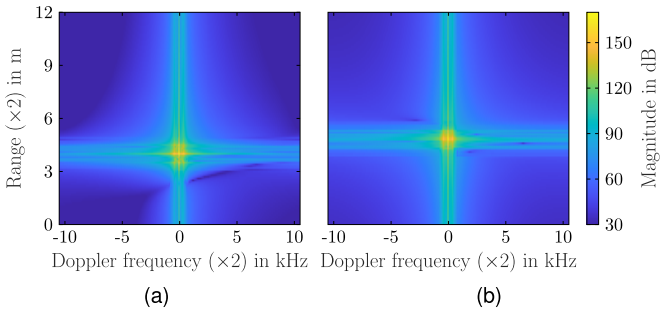

Fig. 6. Range-Doppler map of a single static target at 2 m distance, tagged with 5 kHz and after removal of the Doppler tag influence from (a) simulations and (b) measurements. Range and Doppler are doubled in comparison to Fig. 5 due to the multiplication in (7); however, for static targets, the effect is only visible in range.

itself, not only the artificial frequency shift f_{id} but also the unknown phase shift φ_{id} are canceled out so that the phase offset of the radar signal φ_b is not corrupted by the Doppler tag operation. This is even the case if the artificial frequency shift is not exactly known. Consider a deviation in the applied f_{id}, $f_{\mathrm{id}} + \Delta$, e.g., due to nonideal tag components. Identification is not impaired as long as the resulting frequency shift can still be assigned to the original f_{id}, which should be ensured using guard intervals. Equation (5) will change accordingly, but nonetheless, the same frequency shift $f_{\mathrm{id}} + \Delta$ occurs in both sidebands and can be eliminated equivalent to (7), given that the windows still contain at least most of the tag-caused signal components. This is also evident from the fact that the knowledge of possible $f_{\mathrm{id},x}$ is used only for identification and window placement, not for any subsequent processing.

Fig. 7 contains a cut through Fig. 6 in the Doppler direction to illustrate the elimination of the Doppler tag influence but also highlight remaining tag- and windowing-caused Doppler components that impede range estimation.

If the Doppler elimination is not sufficient or if the tagged object is in motion, an additional Doppler correction can be applied. The Doppler shift is estimated using an FFT and subsequent chirp Z transform (CZT) and used for the correction of all v-dependent terms in (4). The concept was introduced in [22] and, considering the factor of 2 for velocity estimation, is applicable to a radar-tag system without modifications. Thus, all remaining Doppler shifts are corrected as if they were motion-caused. An error occurs due to the correction of the left-over tag shift as motion-caused Doppler but is negligible as these tag-caused Doppler shifts are very small. Therefore,

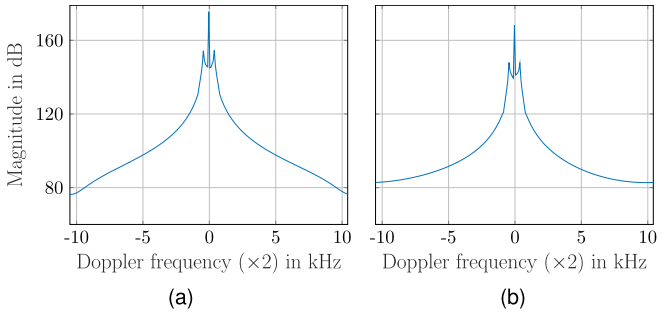

Fig. 7. Doppler profile of a single static target at 2 m distance, tagged with 5 kHz and after removal of the Doppler tag influence from (a) simulations and (b) measurements.

the additional Doppler correction is generally beneficial and applied hereinafter.

Together with the cancellation of the unknown mixing phase shift φ_{id}, this allows for a reliable evaluation of the phase offset for range estimation in addition to the frequency-based analysis as in [21]. This combined analysis can only be used if a suitable hardware approach and corresponding preprocessing ensure the elimination of any tag influence in frequency and phase. It utilizes the fact that two independent range estimates can be gained from the radar signal. The first coarse one determines the range bin of interest, while the second one is used to estimate the range with high accuracy within this bin. All chirps of the FC-FMCW frame are summed up to a single one prior to range estimation so that the complete processing gain of all chirps is exploited. This is fine after Doppler tag removal and Doppler correction because each chirp then contains the same information about the range at the beginning of the measurement. Although Doppler-FFT and -CZT are used to estimate the Doppler, the corresponding processing gain would otherwise not be included in the range estimation. The coarse, frequency-based range estimate R_f is obtained from the first term of (9) using an FFT, followed by a CZT to reach higher accuracy. It is used to determine a first estimate for the delay $\widehat{\tau}_0$ and choose the range bin of interest by means of the number of complete phase rotations corresponding to the target range. The second estimate R_φ is determined from the phase offset of the radar signal φ_b and reaches higher accuracy but is only unambiguous within 2π. The phase offset is attained from the complete signal phase $\Phi_{b,w/o\,t}$ by an elimination of the estimated frequency term $2\pi(B/T)\widehat{\tau}_0 \cdot t$, realized as the multiplication with an inverted exponential term. The same elimination is used for the quadratic term $-2\pi(B/2T)\widehat{\tau}_0^2$ so that

$$s_{\mathrm{b,corr}} = e^{j\Phi_{\mathrm{b,w/o\,t}}} \cdot e^{-j2\pi\frac{B}{T}\widehat{\tau}_0 \cdot t} \cdot e^{j2\pi\frac{B}{2T}\widehat{\tau}_0^2} \tag{10}$$

results in

$$\varphi_{\mathrm{b,corr}} = 2\pi \cdot \tau_0 f_{\mathrm{min}}. \tag{11}$$

Using (11) and (3) and assuming $v = 0\ \mathrm{m\,s^{-1}}$, R_φ can be determined to be

$$R_\varphi = \frac{c_0}{4 f_{\mathrm{min}}} \frac{\varphi_{\mathrm{b,corr}}}{\pi}. \tag{12}$$

If the correct range bin is chosen using R_{f}, R_φ is used to determine a highly accurate range estimate R_{fin} within this

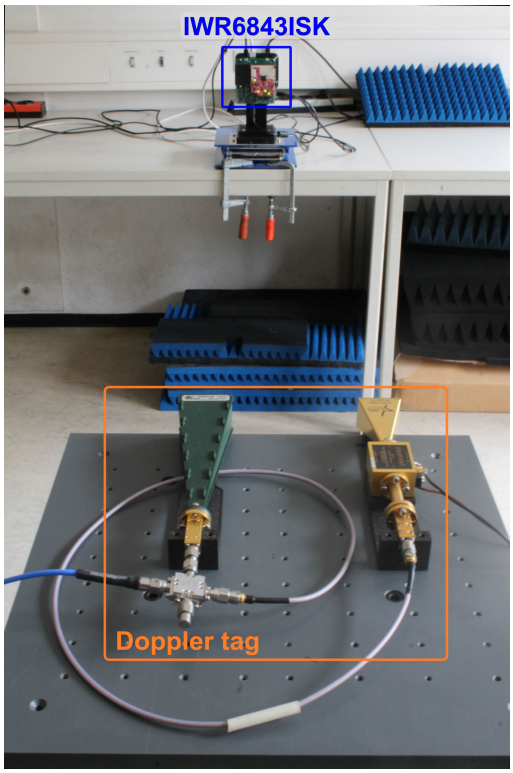

Fig. 8. Measurement setup with the radar sensor facing the Doppler tag in its most basic version.

bin, hence combining high accuracy and large unambiguous range from the two estimates to be

$$R_{\text{fin}} = \left\lfloor \frac{2f_{\text{min}}}{c_0} \cdot R_{\text{f}} \right\rfloor \cdot \frac{c_0}{2f_{\text{min}}} + R_{\varphi}. \tag{13}$$

Only the additional, but constant factor of 2 from (5) has to be considered; hence, the correct range estimate is $(R_{\text{fin}}/2)$, and the unambiguous range is only half its original size.

Using complex mixing, only one sideband is present. The frequency shift is estimated for identification and can be corrected, but the phase shift remains unknown and impedes phase offset analysis. Hence, only the less accurate frequency-based range estimation is applicable in this case. More attention has to be paid to potential velocities of the tagged objects as those apply a frequency shift not separable from the one caused by the Doppler tag. Hence, guard intervals with a velocity-dependent width are to be kept free around each tag to allow for the identification of tagged objects in motion. This can be challenging if the expectable velocities are unknown and additionally limits the available number of tags.

III. Measurements Demonstrating Identification and Range Estimation Capabilities

The performance of the proposed Doppler tag is demonstrated in measurements investigating both the identification capabilities of the tag as well as the achieved range estimation accuracy. The general measurement setup is shown in Fig. 8. A Doppler tag, composed of off-the-shelf RF components, faces a commercial radar sensor. The Doppler tag is designed

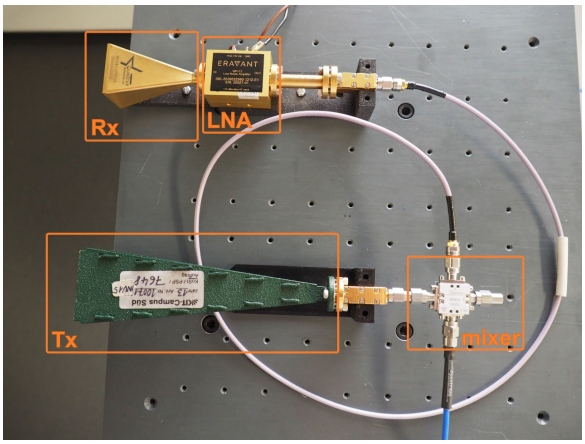

Fig. 9. Doppler tag setup with Rx antenna (22.5 dBi gain), LNA (25 dB gain, 6 dB noise figure), double-sideband mixer (12 dB noise figure), and Tx antenna (25 dBi gain).

TABLE I
Measurement Parameters for IWR6843ISK

Minimum frequency f_{min}	60 GHz
Sampled bandwidth B	1.5 GHz
Sampled chirp duration T	32 µs
Number of samples per chirp N_{sample}	256
Number of chirps N_{chirp}	255
Range resolution ΔR	0.1 m
Maximum unambiguous range R_{max}	12 m
Velocity resolution Δv	0.2 m/s
Maximum unambiguous velocity v_{max}	26 m/s
Maximum unambiguous Doppler frequency $f_{\text{D}_{\text{max}}}$	10.5 kHz

for operation in the extended E-band at around 60 GHz. The frequency was chosen in an ISM band and as a compromise between available bandwidth for range estimation and path attenuation. In a first setup, the tag consists only of the receive and transmit antennas, an LNA with 25 dB amplification, and an IQ mixer, of which the I port is terminated to enable real-valued mixing. The local oscillator (LO) port of the mixer is connected to the receive path of the tag, and an artificial Doppler frequency f_{id} is applied at the Q port, allowing the usage and investigation of different $f_{\text{id},x}$. No PA is used by now, and it is ensured that neither the incoming radar signal saturates the tag nor does the tag response saturate the radar. The setup is fixed to a platform so as not to move. Fig. 9 provides a closer look at this Doppler tag setup. The used radar sensor is an IWR6843ISK from Texas Instruments with the measurement parameters given in Table I, also fixed to avoid motion in the setup as a purely static scenario is considered. Absorber material is used to suppress reflections from metal parts in the background as well as multiple reflections. 300 measurement iterations are conducted for most investigations, and the results shown are the mean values of those, if not stated differently.

A. Target Identification Using a Doppler Tag

To investigate the identification capabilities of the tag and possible influence factors, a number of measurement series are

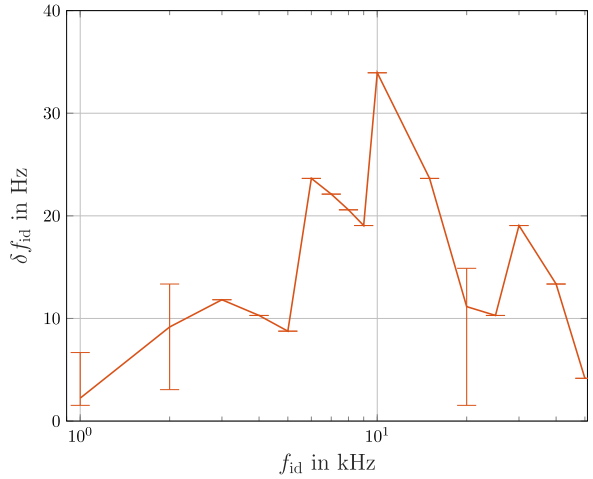

Fig. 10. Mean of absolute identification frequency error over applied identification frequencies, including minimum and maximum values as error bars.

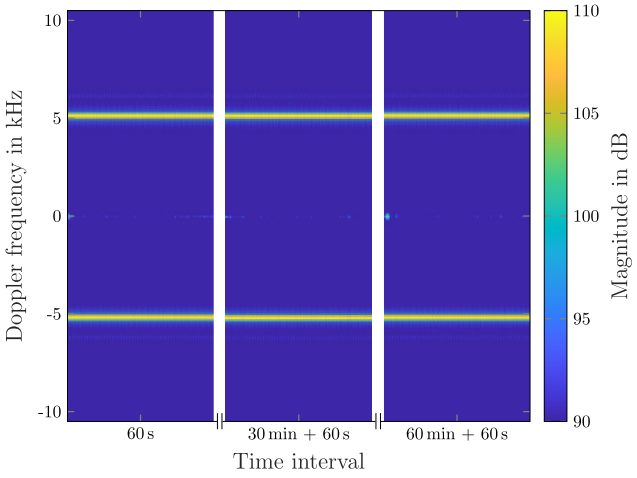

Fig. 11. Results of a STFT showing the tag frequency in three time intervals of 60 s with 30 min in between. The Doppler tag is turned on during the whole time.

conducted. In Fig. 10, the deviation of the estimated identification frequency $\widehat{f_{\mathrm{id}}}$ to the actually applied f_{id}, $\delta f_{\mathrm{id}} = |\widehat{f_{\mathrm{id}}} - f_{\mathrm{id}}|$, is shown in dependency of f_{id}. The signal generator used to generate f_{id} is validated by measurement in accuracy and stability over time to serve as a reference. The found generator error is at least one order of magnitude below the errors occurring in Fig. 10 for all used frequencies and can hence be omitted. The distance between radar and tag is kept at a constant value of around 2 m, and the depicted δf_{id} is the mean value of 300 iterations of the same measurement for each f_{id}. The mean absolute error (MAE) is used not to influence results by canceling values; hence, only positive values are found. Additionally, the minimum and maximum deviations within these 300 iterations, $\delta f_{\mathrm{id,min/max}}$, are depicted as error bars. The achieved identification accuracy is shown to be relatively stable up to high f_{id}, so that multiple objects with different $f_{\mathrm{id},x}$ can be comparably identified. Only a slight tendency toward higher identification frequency errors is observed for higher f_{id} within the maximum unambiguous frequencies, but which are small in relation to the applied $f_{\mathrm{id},x}$. For most $f_{\mathrm{id},x}$, the variance in $\widehat{f_{\mathrm{id}}}$ and hence, δf_{id}, is negligible, only for 1 and 2 kHz, variations are observed. The reason is the influence of the zero-Doppler peak, which is closer for these frequencies than for higher ones. The same holds for 20 kHz, which corresponds to 1 kHz, but in the second Nyquist zone. The maximum occurring $\delta f_{\mathrm{id,max}}$, in dependency of the used $f_{\mathrm{id},x}$, can be utilized to determine a guard interval between consecutive $f_{\mathrm{id},x}$.

Even tag frequencies above the maximum unambiguous frequency can be used, in this case 15–50 kHz, if the overall system design still ensures a unique assignment of tag frequencies to objects. Coupling is not an issue for higher tag frequencies as would be the case for high motion-caused Doppler shifts, for which the coupling terms falsify range estimation. These coupling terms arise from the relation between the Doppler shift and the motion that is causing it. For artificial Doppler shifts introduced by the tag, the influence on the range is eliminated in (7) prior to range estimation, so that the latter is not impaired. In a crowded scenario with many

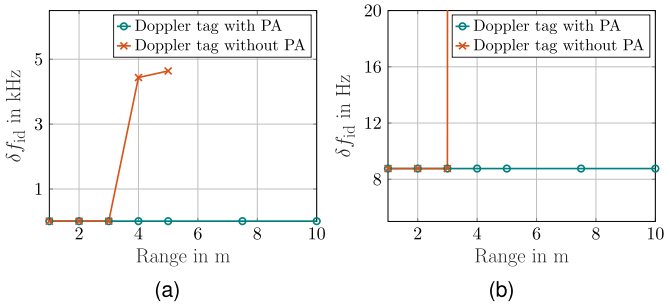

Fig. 12. Mean of absolute identification frequency error over measurement range for a Doppler tag with $f_{\mathrm{id}} = 5$ kHz in a setup with PA (○) and without PA (×). For improved readability, a zoomed version of (a) is shown in (b).

tagged and untagged objects, tag frequencies can therefore be chosen significantly above the expected motion-caused Doppler shifts and with large guard intervals. This simplifies the differentiation between tagged and untagged objects and avoids overlapping of peaks of multiple tagged targets in motion, which would complicate further processing.

To investigate the time-dependency of the Doppler tag, a short-time Fourier transform (STFT) is applied to the measurement results of a tag of $f_{\mathrm{id}} = 5$ kHz over time. Fig. 11 presents the results of the STFT over a time of 1 min, repeated twice with 30 min break in between, during which the Doppler tag is turned on. The identification frequency f_{id} is highly constant over this time, so that solid identification is permanently possible. Together with the first investigation of δf_{id}, this is sufficient to decide on an application-aware guard interval size, dependent on the compromise between reliable object identification and the number of available tag frequencies $f_{\mathrm{id},x}$.

The identification accuracy δf_{id} is further independent of the distance between radar and tag within a tested distance of up to 10 m as long as the tag can be detected. This is shown in Fig. 12, where Fig. 12(b) contains a zoomed-in view in Fig. 12(a). The ranges are measured manually and with low accuracy, as the specific range is not of interest but the invariance of δf_{id} over different ranges. All measurements are

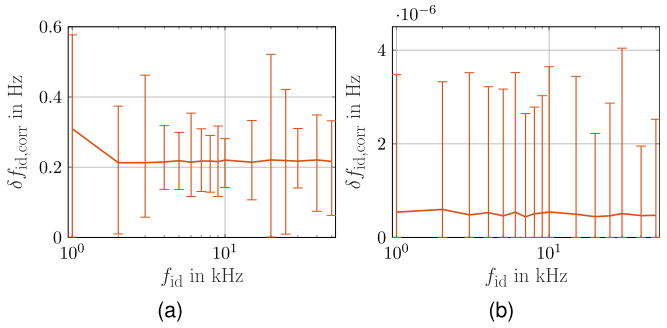

Fig. 13. Mean of absolute identification frequency error over applied identification frequency (a) after Doppler tag removal and (b) after additional Doppler correction, including minimum and maximum values as error bars.

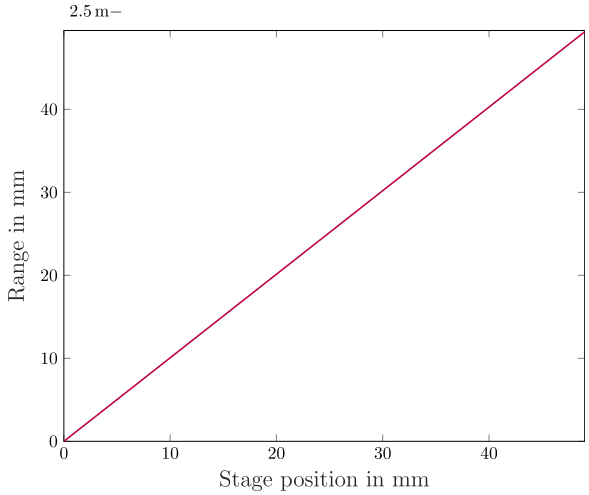

Fig. 14. Estimated range between radar and target over a measurement range of 50 mm for a Doppler tag with $f_{\mathrm{id}} = 5$ kHz. The target starts at a range of 2.5 m and approaches the radar in steps of 1 mm.

conducted with a tag frequency of $f_{\mathrm{id}} = 5$ kHz, and again, the mean of 300 iterations is shown. In the basic Doppler tag setup, identification is unaffected up to a range of 3 m. Beyond, the tag response is too weak and mostly undetectable due to a low signal-to-noise ratio (SNR), so identification is deteriorated or even impossible. The error of nearly 5 kHz implies that in most of the 300 iterations, the tag was not detected and a tag frequency of 0 Hz is determined, leading to $\delta f_{\mathrm{id}} = f_{\mathrm{id}}$. Adding a PA to the transmit path of the tag can be beneficial for range estimation but does not influence the identification accuracy as also shown in Fig. 12 for an amplifier gain of 27 dB. There is hence no proportional connection between SNR and identification accuracy so that δf_{id} is at the same value of 8.8 Hz for both Doppler tag setups, and as also visible in Fig. 10 at $f_{\mathrm{id}} = 5$ kHz. However, due to the amplification of the tag response, the range up to which the tag can be reliably detected and identified expands. Guard intervals are consequently neither range nor SNR dependent; as long as the tag is detected, the identification frequency error is stable, and if the tag cannot be detected anymore, identification is not possible, and guard intervals are not applicable.

After successful identification, the applied Doppler shift has to be removed to allow for unimpaired range estimation. As discussed in Section II-B, the two sidebands are separated and then multiplied to eliminate both frequency shift and phase shift originating from the tag operation. Remaining Doppler components in the signal would result in an offset in range estimation, hence decreasing the estimation accuracy. Ideally, no tag influence is left after elimination, and only static targets remain for range estimation. This was already shown in Fig. 6 for an exemplary measurement and is confirmed in Fig. 13(a), where frequency and phase shift are removed from the measurements of Fig. 10. $\delta f_{\mathrm{id,corr}}$ describes the deviation of a Doppler estimation after removal from the expected value of $f_{\mathrm{id,corr}} = 0$ Hz. The results are close to zero over all $f_{\mathrm{id},x}$, which proves a successful elimination of the tag influence. An additional Doppler correction as discussed in Section II-B, using an estimation of the remaining Doppler shift after tag elimination, improves the tag elimination and leaves purely static signal components as shown in Fig. 13(b). Therefore, the static-target requirement for high-accuracy range estimation as described in Section II-B is fulfilled.

B. High-Accuracy Range Estimation

To investigate range estimation, the setup is modified to include an M-683 Piezo Motorized Precision Translation Stage from Physik Instrumente, which allows for small-step adjustment of the range between radar and tag. Fig. 14 contains the range estimation over a measurement range of 50 mm in steps of 1 mm. The target starts at the largest distance and approaches the radar step by step, but is static during each measurement. At the first position, the estimated range between radar and target is around 2.5 m. To determine the accuracy of range estimation, the true range is to be known accurately to serve as a reference. The radar is not calibrated in the discussed setup, and no absolute reference system is available; hence, relative measurements are conducted to provide reference, so that each measurement refers to a reference measurement. The range error δR_{fin} is calculated as the deviation of the range estimates of these two measurements. The underlying signal processing steps are performed as discussed in II-B. The signal propagation time within the tag is assumed to be constant and does hence not influence the measurements due to their relative manner. For absolute measurements, this time had to be considered during radar calibration.

The range error over a measurement range of 50 mm in steps of 1 mm is shown in Fig. 15 as the MAE of 300 measurement iterations. Additionally, minimum and maximum errors are depicted as error bars. The absolute distance between radar and target is around 2 m. To provide a direct comparison, the error is displayed for a Doppler tag with $f_{\mathrm{id}} = 5$ kHz as radar target as well as a simple corner reflector of side length 14 cm ($\approx$18 dB m^2). The range error and its variance using a Doppler tag are smaller than the ones using a corner reflector. This can be explained as the accuracy of range estimation generally depends on the SNR in the measurements, which is higher for the active Doppler tag. In addition, the measurement surrounding is effectively suppressed during Doppler tag removal, further enhancing the range estimation. The influence of the Doppler tag beyond these enhancements is successfully eliminated and therefore does not impede range estimation.

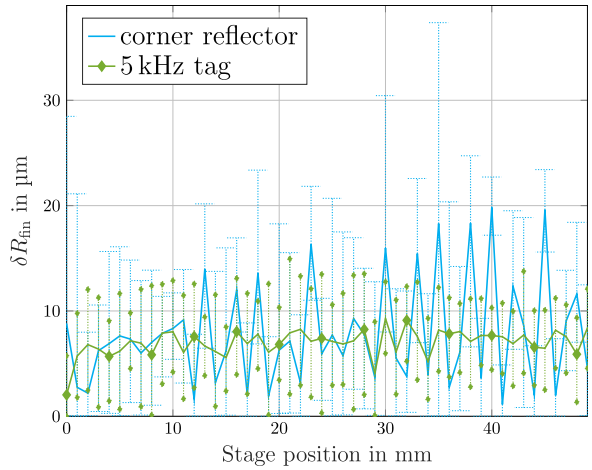

Fig. 15. Mean of absolute range error δR_{fin} over a measurement range of 50 mm for a Doppler tag with $f_{\text{id}} = 5$ kHz (♦) and a corner reflector (—) as radar target. The absolute distance between radar and target is around 2 m. Minimum and maximum values are included as error bars (⋯).

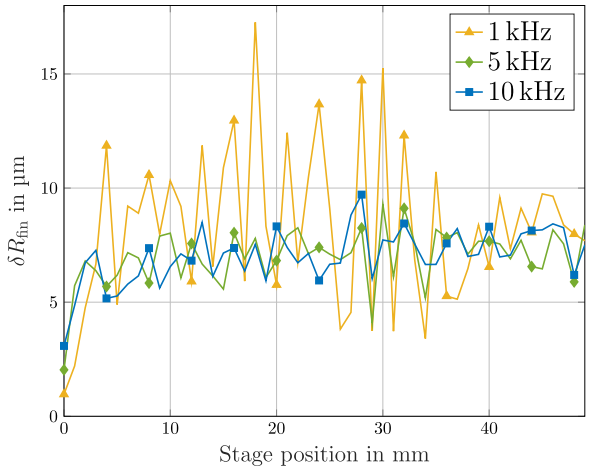

Fig. 16. Mean of absolute range error δR_{fin} for applied identification frequencies of 1 kHz (▲), 5 kHz (♦), and 10 kHz (■).

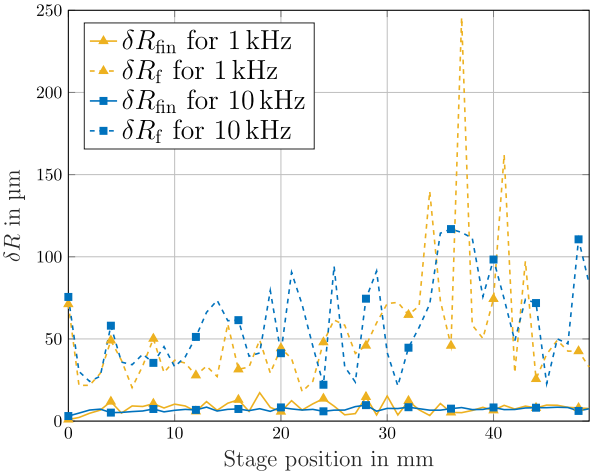

Fig. 17. Mean of absolute range error for $f_{\text{id}} = 1$ kHz (▲) and $f_{\text{id}} = 10$ kHz (■) for combined range estimation δR_{fin} (—) and frequency-based range estimation δR_f (– –).

Fig. 16 presents the investigation of the achieved range error for three different tag frequencies f_{id}. For each $f_{\text{id},x}$, an investigation as shown in Fig. 15 is performed. The range error for $f_{\text{id}} = 1$ kHz is slightly larger than for the other frequencies and also contains larger variations. The reason is again the influence of the zero-Doppler peak, which was not completely suppressed. However, the achieved accuracy is still high and a significant improvement compared to the accuracy of frequency analysis as contrasted in Fig. 17 for 1 and 10 kHz. Not only the mean range error but also its variations can be considerably reduced with the combined analysis. No significant influence of the tag frequency can be read from the results, so range estimation with comparable accuracy can be performed for all tagged objects in a scenario.

Irrespective of the tag frequency, the range error is expected to be range-dependent, which is mainly referable to the change in SNR. By adding a PA to the transmit path of the tag, the SNR and, therefore, accuracy can be enhanced. Particularly for large distances, the target peak can be amplified to rise above the noise floor that would otherwise hide it as found in Fig. 12. For small distances, the accuracy may remain or even drop as not only the intended target peak is enlarged but also multiple reflections, which distort range estimation. It hence depends on the actual application if an improvement can be accomplished using an additional PA and if it justifies the more complex tag setup. Fig. 18 contains the achieved range error for measurement ranges of up to 10 m using a Doppler tag setup with $f_{\text{id}} = 5$ kHz and including a PA with 27 dB gain. The shown error is the MAE of 300 iterations at each of the seven measurement positions. Within this range, no tendency toward higher range errors is observed; the error is stable. However, the minimum and maximum error values, depicted as error bars, increase with higher ranges; hence, outliers are more likely, and the estimation becomes less reliable for larger distances.

This can also be observed in Fig. 19, where the range error over ranges of up to 10 m is depicted again and for the same tag setup, this time as the MAE of 300 measurement iterations at 50 stage positions, so 15 000 measurements are averaged. With the variation in measurement position and the large number of measurements, outliers are likely to be included if they occur. In Fig. 19, this is the case starting from 4 m and for all subsequent measurements. Mostly, an erroneous bin is chosen so that an error of the size of one bin ($c_0/(2f_{\text{min}}) = 2.5$ mm) occurs. More frequent bin errors consequently raise the mean error as only absolute values are considered. In addition to the results of a combined range estimation, the range error after frequency analysis is shown. The comparison of both curves indicates that phase analysis can only significantly enhance range estimation up to a relatively small range of around 3 m; beyond that, frequency and combined analysis result in similar range errors. This is because the combined analysis relies on the frequency analysis for bin selection and phase correction, and the phase analysis is more sensitive to a low SNR.

Therefore, combined analysis is most suitable for short ranges, whereas frequency analysis can provide comparable range estimation over large distances. This is also compliant with the typical requirements, as high accuracy is mostly

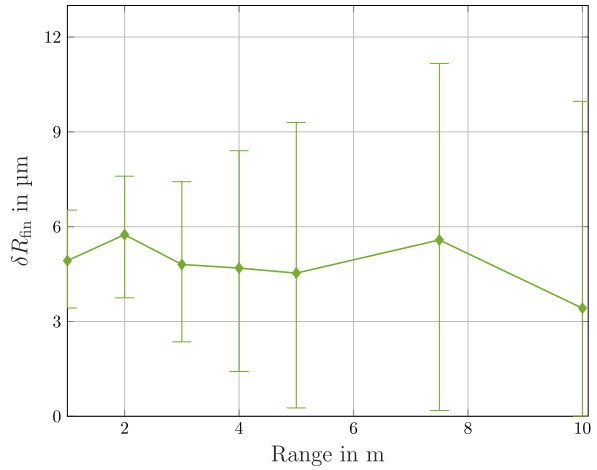

Fig. 18. Mean of absolute range error δR_{fin} over measurement range for a Doppler tag with $f_{\text{id}} = 5$ kHz, including minimum and maximum values as error bars.

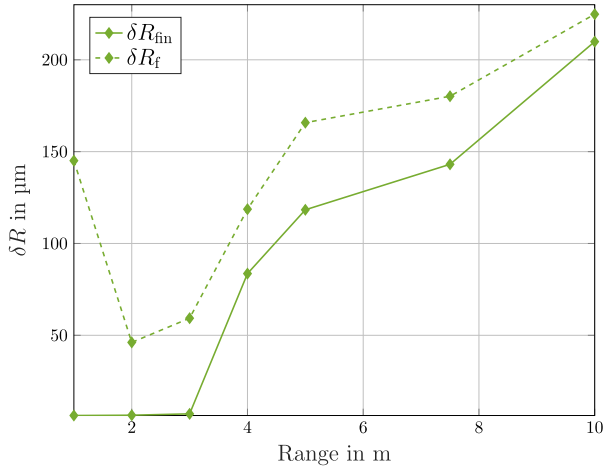

Fig. 19. Mean of absolute range error over measurement range for a Doppler tag with $f_{\text{id}} = 5$ kHz. The mean is determined over 300 measurement iterations and 50 stage positions per range. Results are depicted for combined range estimation δR_{fin} (—) and frequency-based range estimation δR_f (– –).

requested in close proximity, while at a distance of several meters, mm-accuracy is sufficient for most applications. A combination of both approaches with range-dependent processing decision can reduce computational effort and still benefit from exceptionally high accuracy where needed. The Doppler tag can, in addition to identification, enlarge the operational range with appropriate amplification and allow for efficient static target suppression during processing. It does, hence, support (high-accuracy) range estimation for the tagged objects, while no negative influence on the estimation was observed.

IV. Conclusion

The idea of a Doppler tag to uniquely identify objects with conventional radar hardware and estimate their range with high accuracy was introduced. The proposed combination of hardware and signal processing enables a complete overview of the surroundings, with simultaneous identification of tagged objects and high-accuracy range estimation as well as velocity estimation for tagged as well as untagged objects. This article presented the underlying system and processing model along with a realization of the tag using commercial components in conjunction with an off-the-shelf radar sensor. The tag's capabilities in terms of identification and accompanying range estimation were investigated. Hardware and processing requirements for high-accuracy range estimation were discussed, and measurements showcased the achievable accuracy in terms of range error and minimum and maximum deviations, all in the μm range. Identification and range estimation accuracy were shown to be independent of the used tag frequencies, so that multiple objects can be supplied and experience comparable performance. The range dependency as well as scenario-aware setup modifications were discussed in both cases. In summary, unique and robust object identification was achieved while a very high range estimation accuracy was preserved. The investigations provide a comprehensive overview of what can be accomplished in radar systems using a Doppler tag.

Acknowledgment

The authors would like to thank Texas Instruments for providing the radar sensor.

References

[1] A. D. Semenov, H. Richter, U. Bottger, A. V. Smirnov, and H.-W. Hubers, "Distant detection of hidden objects with a THz imaging radar," in *Proc. Joint 32nd Int. Conf. Infr. Millim. Waves 15th Int. Conf. THz Electron.*, Sep. 2007, pp. 652–653.

[2] S. Ayhan, S. Scherr, A. Bhutani, M. Pauli, and T. Zwick, "Radar sensor for waveguide based distance measurements in machine tool components," in *IEEE MTT-S Int. Microw. Symp. Dig.*, Apr. 2015, pp. 1–4.

[3] M. Vossiek, R. Roskosch, and P. Heide, "Precise 3-D object position tracking using FMCW radar," in *Proc. 29th Eur. Microw. Conf.*, Oct. 1999, pp. 234–237.

[4] H. M. Aumann and N. W. Emanetoglu, "A wideband harmonic radar for tracking small wood frogs," in *Proc. IEEE Radar Conf.*, May 2014, pp. 108–111.

[5] X. Gao, A. Singh, O. Boric-Lubecke, and V. M. Lubecke, "Small-scale displacement measurement with passive harmonic RF tag using Doppler radar," in *Proc. IEEE Int. Wireless Symp. (IWS)*, Apr. 2013, pp. 1–4.

[6] A. Singh and V. Lubecke, "A heterodyne receiver for harmonic Doppler radar cardiopulmonary monitoring with body-worn passive RF tags," in *IEEE MTT-S Int. Microw. Symp. Dig.*, May 2010, pp. 1600–1603.

[7] S. Hansen, C. Bredendiek, G. Briese, and N. Pohl, "A compact harmonic radar system with active tags at 61/122 GHz ISM band in SiGe BiCMOS for precise localization," *IEEE Trans. Microw. Theory Techn.*, vol. 69, no. 1, pp. 906–915, Jan. 2021.

[8] N. Nourshamsi, S. Vakalis, and J. A. Nanzer, "Joint detection of human and object motion using harmonic micro-Doppler radar and harmonic tags," *IEEE Antennas Wireless Propag. Lett.*, vol. 19, pp. 930–934, 2020.

[9] E. Sippel et al., "Quasi-coherent phase-based localization and tracking of incoherently transmitting radio beacons," *IEEE Access*, vol. 9, pp. 133229–133239, 2021.

[10] W. Kang, S. Xu, and W. Wu, "Time-division multiple tags based multitarget respiration monitoring radar with a single beam," *IEEE Microw. Wireless Compon. Lett.*, vol. 32, no. 2, pp. 181–184, Feb. 2022.

[11] J. Thornton and D. J. Edwards, "Range measurement using modulated retro-reflectors in FM radar system," *IEEE Microw. Guided Wave Lett.*, vol. 10, no. 9, pp. 380–382, Sep. 2000.

[12] M. Cohn, "A millimeter wave retrodirective transponder for collision/obstacle avoidance and navigation/location," in *Proc. VNIS Vehicle Navigat. Inf. Syst. Conf.*, Oct. 1993, pp. 534–538.

[13] I. Cnaan-On, S. J. Thomas, J. L. Krolik, and M. S. Reynolds, "Multichannel backscatter communication and ranging for distributed sensing with an FMCW radar," *IEEE Trans. Microw. Theory Techn.*, vol. 63, no. 7, pp. 2375–2383, Jul. 2015.

[14] X. Fu, A. Pedross-Engel, D. Arnitz, C. M. Watts, A. Sharma, and M. S. Reynolds, "Simultaneous imaging, sensor tag localization, and backscatter uplink via synthetic aperture radar," *IEEE Trans. Microw. Theory Techn.*, vol. 66, no. 3, pp. 1570–1578, Mar. 2018.

[15] A. Strobel and F. Ellinger, "An active pulsed reflector circuit for FMCW radar application based on the switched injection-locked oscillator principle," in *Proc. Semiconductor Conf. Dresden*, Sep. 2011, pp. 1–4.

[16] F. R. Williamson, L. F. Moore, R. Brooks, J. A. Williamson, and M. C. McGee, "A coded radar reflector for remote identification of personnel and vehicles," in *Proc. Rec. IEEE Nat. Radar Conf.*, Apr. 1993, pp. 186–191.

[17] T. Iizuka, T. Sasatani, T. Nakamura, N. Kosaka, M. Hisada, and Y. Kawahara, "MilliSign: mmWave-based passive signs for guiding UAVs in poor visibility conditions," in *Proc. 29th Annu. Int. Conf. Mobile Comput. Netw.* New York, NY, USA: Association for Computing Machinery, Oct. 2023, pp. 1–15, doi: 10.1145/3570361.3613264.

[18] A. Jiménez-Sáez et al., "Frequency selective surface coded retroreflectors for chipless indoor localization tag landmarks," *IEEE Antennas Wireless Propag. Lett.*, vol. 19, pp. 726–730, 2020.

[19] A. A. Abbas, Y. Zantah, A. Abuelhaija, and T. Kaiser, "Millimeter-wave retro-directive frequency coded lens by curved one-dimensional photonic crystal resonator," *IEEE Access*, vol. 10, pp. 132988–133000, 2022.

[20] S. Scherr, S. Ayhan, J. Hofmann, M. Pauli, and T. Zwick, "Sweep time variation algorithm for high accuracy FMCW radar measurements," in *Proc. German Microw. Conf.*, Mar. 2015, pp. 182–185.

[21] T. Antes, Z. Kollár, T. Zwick, and B. Nuss, "High-accuracy range estimation for FC-FMCW radar using phase evaluation in static scenarios," in *Proc. IEEE Radar Conf. (RadarConf)*, May 2024, pp. 1–6.

[22] T. Antes, Z. Kollár, T. Zwick, and B. Nuss, "Doppler-robust high-accuracy range estimation for FC-FMCW radar," in *Proc. 21st Eur. Radar Conf. (EuRAD)*, Sep. 2024, pp. 79–82.

[23] W. Scheiblhofer, R. Feger, A. Haderer, S. Scheiblhofer, and A. Stelzer, "Simultaneous localization and data-interrogation using a 24-GHz modulated-reflector FMCW radar system," in *IEEE MTT-S Int. Microw. Symp. Dig.*, Jun. 2017, pp. 67–70.

[24] M. S. Dadash, J. Hasch, P. Chevalier, A. Cathelin, N. Cahoon, and S. P. Voinigescu, "Design of low-power active tags for operation with 77–81-GHz FMCW radar," *IEEE Trans. Microw. Theory Techn.*, vol. 65, no. 12, pp. 5377–5388, Dec. 2017.

[25] A. Diewald, T. Antes, B. Nuss, M. Pauli, and T. Zwick, "Range Doppler migration synthesis for realistic radar target simulation," in *Proc. IEEE Topical Conf. Wireless Sensors Sensor Netw. (WiSNeT)*, Jan. 2021, pp. 56–58.

Theresa Antes (Graduate Student Member, IEEE) received the B.Sc. and M.Sc. degrees in electrical engineering and information technology from Karlsruhe Institute of Technology (KIT), Karlsruhe, Germany, in 2018 and 2020, respectively, where she is currently pursuing the Ph.D. degree in electrical engineering (E.E.) with the Institute of Radio Frequency Engineering and Electronics (IHE), with a focus on radar systems.

Her main research interests include enhanced radar signal processing, high-accuracy target parameter estimation with radar, and radar-based object identification.

Paul Schubert received the B.Sc. and M.Sc. degrees in electrical engineering and information technology from Karlsruhe Institute of Technology (KIT), Karlsruhe, Germany, in 2020 and 2023, respectively.

From 2017 to 2023, he worked as a Student Research Assistant at the Institute of Radio Frequency Engineering and Electronics (IHE), KIT. In 2024, he joined Siemens AG, Karlsruhe, as an RF Development Engineer. His research interests include millimeter-wave radar systems and high-accuracy radar signal processing.

Thomas Zwick (Fellow, IEEE) received the Dipl.-Ing. (M.S.E.E.) and Dr.-Ing. (Ph.D.E.E.) degrees from the Universität Karlsruhe (TH), Karlsruhe, Germany, in 1994 and 1999, respectively.

From 1994 to 2001, he was a Research Assistant with the Institut für Höchstfrequenztechnik und Elektronik (IHE), TH. In February 2001, he joined IBM as a Research Staff Member at the IBM Thomas J. Watson Research Center, Yorktown Heights, NY, USA. From October 2004 to September 2007, he was with Siemens AG, Lindau, Germany. During that period, he managed the RF development team for automotive radars. In October 2007, he became a Full Professor with Karlsruhe Institute of Technology (KIT), Karlsruhe. He is currently the Director of the Institute of the Institute of Radio Frequency Engineering and Electronics (IHE), KIT. His research topics include wave propagation, stochastic channel modeling, channel measurement techniques, material measurements, microwave techniques, millimeter-wave antenna design, wireless communication, and radar system design.

Benjamin Nuss (Senior Member, IEEE) received the B.Sc. and M.Sc. degrees in electrical engineering and information technology and the Dr.-Ing. (Ph.D.E.E) degree from Karlsruhe Institute of Technology (KIT), Karlsruhe, Germany, in 2012, 2015, and 2021, respectively.

He is currently working as a Group Leader for radar and communication systems at the Institute of Radio Frequency Engineering and Electronics (IHE), KIT. His work focuses on the development of efficient future radar waveforms and the design of joint communication and sensing systems. His current research interests include orthogonal frequency-division multiplexing-based multiple-input multiple-output radar systems for future automotive and industrial applications.

Dr. Nuss has authored and co-authored the best publication of 2021 and 2022 within the ITG Society, which was awarded the VDE ITG Prize.